In previous studies, the area of hemolysis analyzed by CFD was limited to the impeller area of the pump, and recirculation and turbulence behind the impeller were not considered. In this study, we therefore analyzed the fluid dynamics in the whole axial flow pump. The aims of this study were to determine fluid dynamics in the whole intra-cardiac axial flow pump and to verify the accuracy of prediction of hemolysis based on CFD analysis by comparing results of CFD analysis with in vitro experimental results.

MATERIAL AND METHODS

Axial flow pump

The axial flow pump consists of a direct current brushless motor, an impeller, and a guide vane. The motor and impeller assembly is fixed to a stainless-steel casing via the guide vane. The casing is a cylinder of 38 mm in diameter with an inlet of 15 mm in diameter and an outlet of 15 mm in diameter. The motor casing is equipped with a semispherical cap to prevent swirling. A spacer is fixed to the motor housing between the impeller and the motor housing to reduce stagnation of flow. The motor is housed in a stainless-steel cylindrical casing of 22 mm in outer diameter and 30 mm in length. Four different impellers were used in this study. The structures of the four-vane impellers are shown in Fig. 1. Each impeller has four vanes with an outer discharge angle of 19.2°. The outer diameter of the impeller is 22 mm, and the hub diameter is 13 mm. Radial clearance between the impeller and the housing is 0.5 mm. A four-vane two-stage impeller was also used. Two four-vane impellers with the same design as that of the above-described four-vane impeller were connected in series. Models of the vane impellers were generated on a computer to satisfy the design parameters (1).

CFD analysis

The software packages Build and TASCflow (Summit AEA Corporation, Tokyo, Japan) were used in this study. The structure of the axial flow pump is shown in Fig. 2. Computational grids were used to solve the full region of the pump. The number of grids was about 127,000. These grids were used to solve the full viscous Reynolds averaged Navier-Stokes equations that were discretized by finite volume elements. The low-Reynolds k-ε turbulent

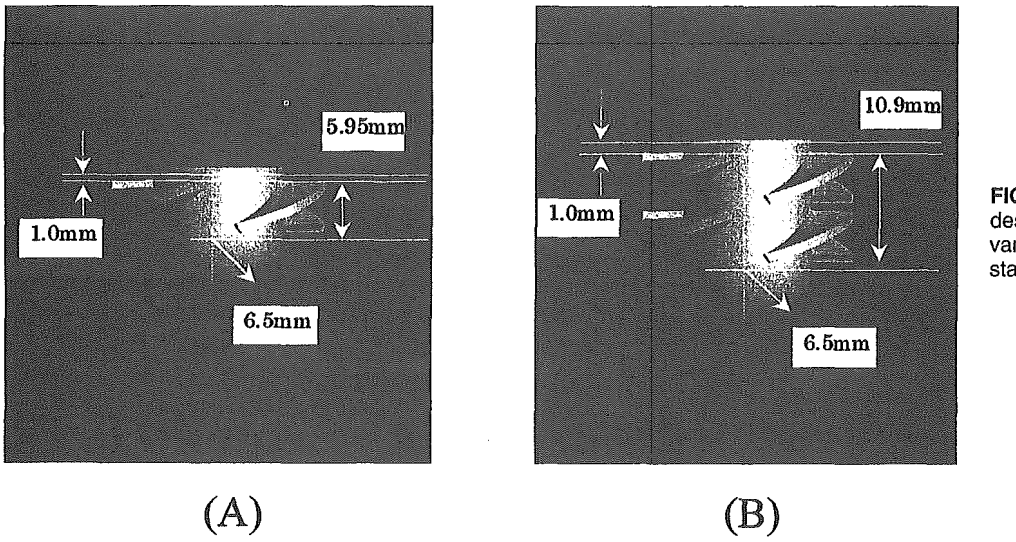

FIG. 1. The drawing shows the design of the impellers: (A) 4-vane impeller, (B) 4-vane 2-stage impeller.

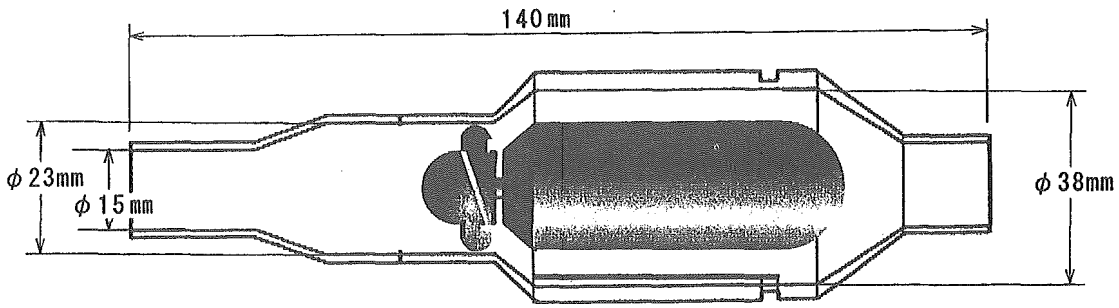

FIG. 2. The figure shows the analyzed area of the axial flow pump.

model was used in these calculations. The boundary conditions were an inlet pressure of 50 mm Hg and an outflow of 5 L/min. The rotational speed of the impeller for each pump was set so as to satisfy the above boundary conditions. Frozen-rotor computations were used to calculate the stationary parts and the rotating part at the same time.

For evaluation of pump performance, fluid density and viscosity were set at 998.2 kg/m^3 and 0.993 mPa·s, respectively, the same as those of water. For prediction of hemolysis, fluid was assumed to be Newtonian fluid having a density of 1,060 kg/m^3 and a viscosity of 3.6 mPa·s.

Calculation of shear stress value of the flow field

Mechanisms of blood damage and effects of shear stress on blood corpuscles were investigated by Giersiepen et al. (8). They assessed blood damage as a function of shear stress applied to erythrocytes. The following basic model for estimation of blood damage is proposed:

$$\mathrm{dHb/Hb[\%]} = 3.62 \times 10^{-5} \times t^{0.785} \times \tau^{2.416}, \quad (1)$$

where Hb is hemoglobin content, dHb is damaged hemoglobin content, t is exposed time [s], and τ is shear stress [N/m^2].

TASCflow can provide the components of the Reynolds stress tensor as scalar parameters.

The Reynolds stress tensor components are described by the following equation:

$$\overline{\rho u'_i u'_j} = -\frac{2}{3}\rho k \delta_{ij} + \mu_t\left(\frac{\partial u_i}{\partial x_j} + \frac{\partial u_j}{\partial x_i}\right), \quad (2)$$

where μ_t is the fluid turbulent viscosity, u' is the fluctuating component of the fluid mean velocity, and δ is the Kronecker's symbol. TASCflow provides these values as s_{ij_turb} at each node.

Molecular shear stress was obtained by calculating the gradient of velocity from Eq. 2:

$$\sigma_{ij} = \mu\left(\frac{\partial u_i}{\partial x_j} + \frac{\partial u_j}{\partial x_i}\right). \quad (3)$$

The shear stress in the turbulent flow was obtained as a summation of the molecular and Reynolds shear stresses.

$$\tau_{ij} = \sigma_{ij} + s_{ij}. \quad (4)$$

Using the method proposed by Bludsuweit (9), the scalar stress value at any point within the six components of the overall stress tensor was given as

$$\tau = \left[\frac{1}{6}\sum(\tau_{ii} - \tau_{jj})^2 + \sum \tau_{ij}^{\,2}\right]^{\frac{1}{2}}. \quad (5)$$

Estimation of shear stress acting on a particle

Using the particle tracking command of TASCflow, trace data of 50 particles were calculated. The shear stress applied to each particle was calculated from these particle data by referring to the Reynolds shear stress tensor and the fluid turbulent viscosity along the particle trace.

Based on the assumption that the effect of shear stress on red cells is accumulated along the trace, Eq. 1 was summed along the particle trace (10).

It is assumed that the damage parameter D associated with each particle has a value of zero initially (10), when the particle enters into the pump, and increases monotonically due to accumulation of blood damage along the particle trace. When D reaches a value of 1, all particles break.

Increase in the damage of a particle over a period of 0.1 msec is described as follows:

$$d_{p,i} = 3.62 \times 10^{-7} \times \tau_i^{2.416} \Delta t_i^{0.785}, \quad (6)$$

where Δt is time difference between t_i and t_{i+1}.

The damage accumulation from time zero to t_i is given by the following equation:

$$D_{p,i} = D_{p,i-1} + (1 - D_{p,i-1}) d_{p,i}. \quad (7)$$

Hemolysis index is defined as the mean damage of 50 particles:

$$E = \frac{1}{N}\sum_{p}^{N} D_P. \quad (8)$$

Measurements of pump performance in vitro

The axial flow pump was connected to a reservoir bag with silicon tubes (Fig. 3). Saline was used as a working medium. Impeller speed was maintained at 7,000 rpm. Flow rate was changed by compressing the outflow tube with a clamp. The relationship between pump flow and pressure difference across the pump was determined. The flow was monitored with an electromagnetic flowmeter using a 10 mm probe (Model MFV-3200, Tokyo, Japan), and the inlet and outlet pressures were measured by pressure transducers (Model P23XL, Spectramed, Statham, Singapore).

Measurements of hemolysis

The pump was connected to a reservoir bag (volume: 1,000 mL) with silicone tubes (inflow side: 10 mm in inner diameter and 141 cm in length) (Fig. 3). The pump was placed 90 cm below the reservoir bag. Fresh bovine blood (1,000 mL) to which citrate phosphate dextrose had been added was used. The reservoir bag was immersed in a water bath with temperature maintained at 39°C. Outflow resistance

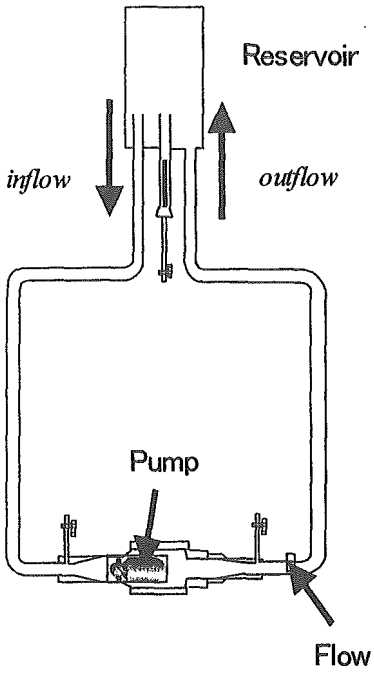

FIG. 3. The experimental set up for hemolysis tests is shown.

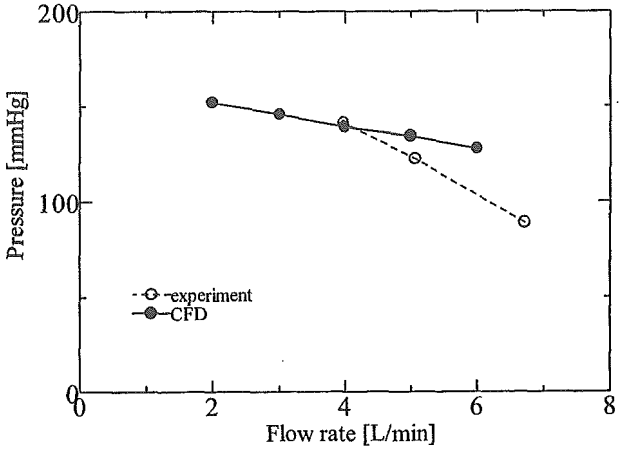

FIG. 4. The graph illustrates HQ characteristics of the axial blood pump.

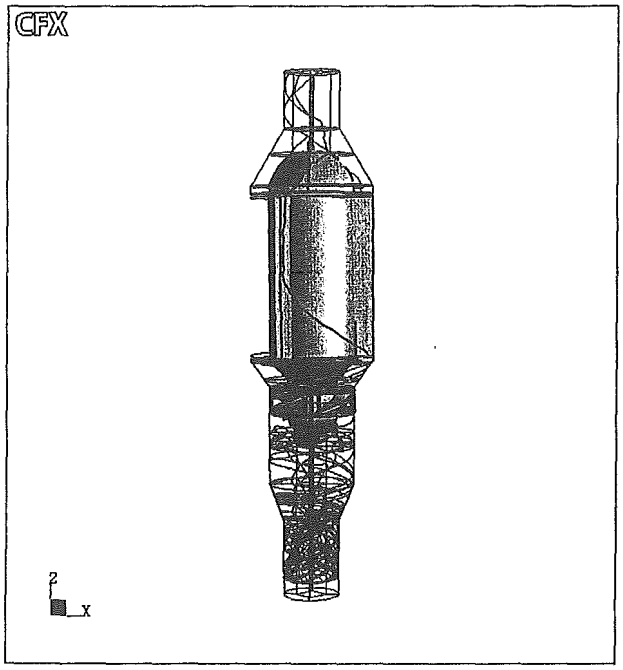

FIG. 5. The diagram shows particle trace lines in the axial flow pump.

was changed by compressing the outflow tube with a clamp. A flow of 5 L/min was maintained for 3 h while keeping the differential pressure at 100 mm Hg. The flow rate, differential pressure, inlet pressure, outlet pressure, and motor speed were recorded by a pen-recorder. Two ml of blood was sampled from the circulating blood and from the control blood every 30 min. The control blood was also kept in the water bath with temperature maintained at 39°C. Free plasma hemoglobin was measured by the tetramethylbenzene method (527-A, Sigma, St. Louis, MO, U.S.A.). The normalized index of hemolysis (NIH) was calculated as follows:

$$\mathrm{NIH} = \Delta\mathrm{freeHb} \times (100 - \mathrm{Ht})/100 \times \mathrm{V} \times 100/(\text{flow time}), \quad (9)$$

where ΔfreeHb is the increase in plasma-free hemoglobin [g/L], V is the blood volume [L], Ht is the hematocrit [%], flow is the pump flow rate [L/min], and time is the sampling interval [min]. Tests were conducted using axial flow pumps with different impellers.

RESULTS

Evaluation of characteristics of the pump

Figure 4 shows a comparison of the pump characteristics determined by CFD analysis and by experiments. The four-vane impeller was driven at 7,000 rpm. The results of CFD analysis agree well with the experimental data at flow rates of less than 4 L/min. However, pressure determined by CFD analysis gradually became lower than that determined by experiments at flow rates above 5 L/min.

Evaluation of hemolysis by CFD analysis

Particle trace lines are shown in Fig. 5. Particles remained in areas in front of the impeller for several rotations of the impeller. Backflow was observed in the clearance region between the impeller and the

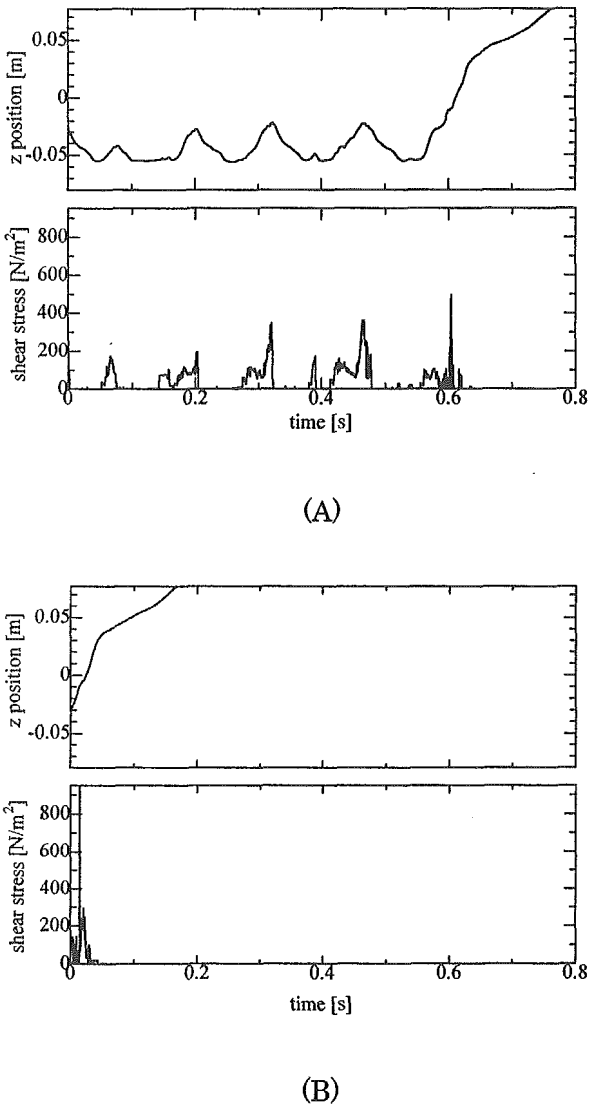

FIG. 6. Changes in the position and stress of a particle in the pump are shown: (A) example of the particle remaining in the impeller region for a long time, and (B) example of the particle passing through the impeller region in a short period.

housing. Figure 6 shows changes in the shear stress along the particle trace in the pump. The particle was exposed to a high shear stress of over 500 Pa when it passed through across the impeller. Another particle remained near the impeller and was exposed to a high shear stress for several rotations of the impeller and then passed out of the pump. Figure 7 shows the mass-weighted distribution of shear stress.

Measurements of hemolysis in vitro

The NIH for each pump is shown in Table 1. To compare the CFD results with the in vitro results, both results were normalized by the value of the 4-vane impeller pump rotating at 8,000 rpm:

$$RIH = \frac{NIH_i}{NIH_B}, \tag{10}$$

$$E_{rel} = \frac{E_i}{E_B}, \tag{11}$$

where NIH_B is the measured NIH of the 4-vane impeller rotating at 8,000 rpm, NIH_i is the measured NIH in other conditions, E_B is the calculated NIH value of model "B" (4-vane impeller rotating at a speed of 8,000 rpm), and E_i is the calculated NIH value in other conditions. Summaries of the results are shown in Figs. 8 and 9. The NIH value of the 4-vane impeller rotating at a speed of 7,500 rpm was lowest in both the results of CFD analysis and the experiments. The 4-vane impeller rotating at 8,000 rpm and the 4-vane 2-stage impeller rotating at 7,000 rpm followed, in the order of low hemolysis. The relative hemolysis value of the 4-vane 2-stage impeller at 8,000 rpm was highest.

DISCUSSION

The choice of flow model is the most important factor in CFD analysis. According to the results of CFD analysis, an area of high turbulence exists around the impeller and areas of low turbulence exist in the inlet and outlet of the pump. When the axial pump is operated at 8,000 rpm in blood, the machine Reynolds number calculated using the impeller diameter is 29830. This value means a relatively low turbulence flow. Therefore, the two-layer low Reynolds k-ε turbulent model was used for calculation of turbulence in this study. Parameters for the wall boundary conditions were decided after performing some preliminary calculations. The calculated pressures at the outlet of the pump agreed well with the experimental data at flow rates of less than 4 L/min. However, the results of CFD analysis became different from the experimental results with increase in flow rate over 4 L/min. A similar tendency was reported by Wood (4). This disagreement was not solved using other turbulence models, and further study is required to solve this problem.

In this study, hemolysis in the axial flow pump was estimated by the equation proposed by Bludszuweit

TABLE 1. *Measured normalized index of hemolysis (NIH)*

	Vane	Gap length [mm]	Speed N [rpm]	NIH
A	4-vane	0.5	7,500	0.028
B	4-vane	0.5	8,000	0.033
C	4-vane 2-stage	0.5	7,000	0.05
D	4-vane 2-stage	1.6	8,000	0.3

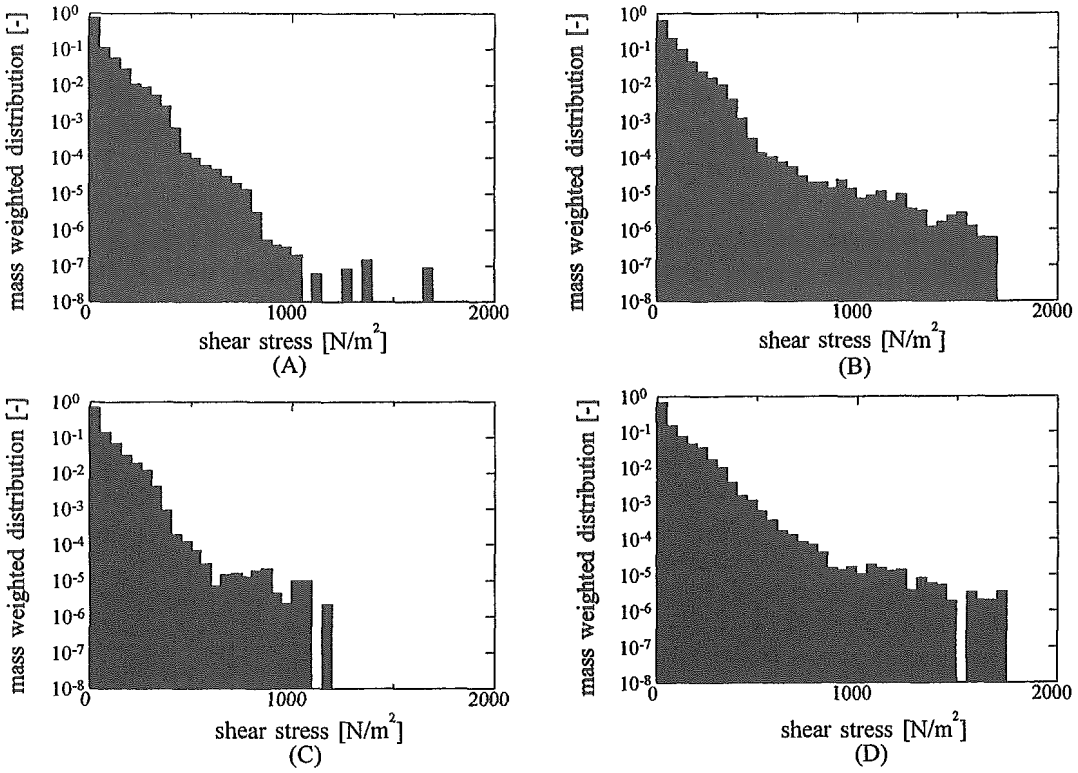

FIG. 7. The mass-weighted distribution of shear stress is illustrated: (A) 4-vane impeller at 7,500 rpm, (B) 4-vane impeller at 8,000 rpm, (C) 4-vane 2-stage impeller at 7,000 rpm, and (D) 4-vane 2-stage impeller at 8,000 rpm.

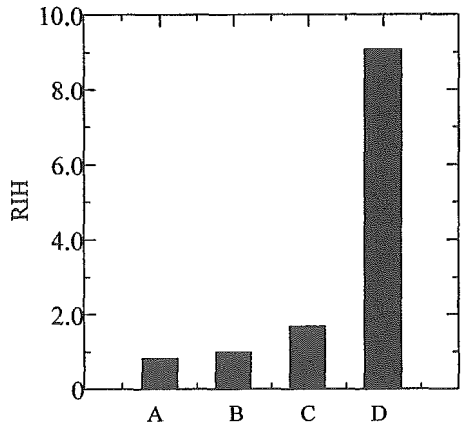

FIG. 8. The graph shows measured relative index of hemolysis (RIH) of various axial flow pumps: (A) 4-vane impeller at 7,500 rpm, (B) 4-vane impeller at 8,000 rpm, (C) 4-vane 2-stage impeller at 7,000 rpm, and (D) 4-vane 2-stage impeller at 8,000 rpm.

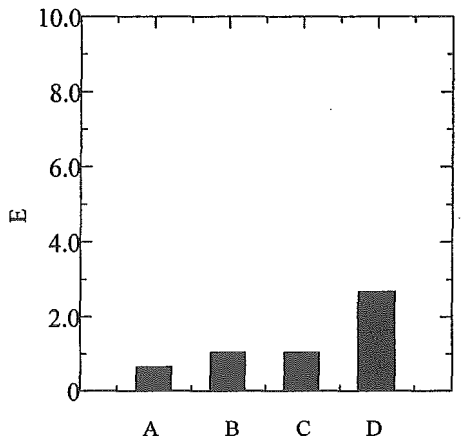

FIG. 9. The graph shows estimation based on CFD hemolysis index (E) of various axial flow pumps: (A) 4-vane impeller at 7,500 rpm, (B) 4-vane impeller at 8,000 rpm, (C) 4-vane 2-stage impeller at 7,000 rpm, and (D) 4-vane 2-stage impeller at 8,000 rpm.

(10) and on the basis of results of CFD analysis. NIH values were estimated by in vitro experiments. The CFD results agreed well with the experimental results for the four-vane impeller, indicating that the estimation of hemolysis by CFD analysis is accurate. However, from a quantitative point of view, the experimental results were different from the results of CFD analysis; the relative index was 9 in the experiment but estimated to be 2.5 by CFD analysis in the case of the 4-vane 2-stage impeller. There are three possible reasons for this difference. First, the

equation proposed by Giersiepen was obtained from a one-dimensional shear stress field using a couette viscometer (8). In the experiments, however, red cells were exposed to three-dimensional shear stress. Second, Giersiepen's equation was obtained for shear stress up to 255 N/m^2 and exposure time of 3–700 ms (8). In the axial pump, there are regions where the shear stress exceeds 1,000 N/m^2 as shown in Fig. 7. In such regions, hemolysis occurs in less than 1 ms (11). Giersiepen's equation was also used to estimate hemolysis for a shear stress of over 1,000 N/m^2. Third, in our hemolysis evaluations, blood was sampled every 30 min from the mock circuit. Hemolysis occurs above a certain level of shear stress (11,12) and generally does not occur at shear stress of less than 150 N/m^2. It is, however, not known whether red cells are destroyed when they are repeatedly exposed to shear stress of less than 150 N/m^2. It is also not known whether the damaged membranes of red cells are restored as time passes. The red cells were repeatedly exposed to high shear stress in the experiments but were exposed to high shear stress only once in the CFD analysis.

Not only hemolysis but also thrombosis is an important problem to be solved for developing a reliable axial blood flow pump. For the development of a blood pump that causes only low rates of hemolysis and thrombosis, regions of high shear stress, back flow, and vortex should be avoided. To achieve this purpose, estimation of shear stress applied to particles using CFD is important.

CONCLUSIONS

Hemolysis in an axial flow pump was measured in in vitro experiments and was also estimated using CFD analysis. A good correlation was found between predicted and measured hemolysis. CFD analysis is useful for developing an atraumatic rotary blood pump.

REFERENCES

1. Mitamura Y, Nakamura H, Okamoto E, Yozu R, Kawada S, Kim DW. Development of the valve pump: An axial flow pump implanted at the heart valve position. *Artif Organs* 1999;23:566–71.
2. Mitamura Y, Nakamura H, Sekine K, Kim DW, Yozu R, Kawada S, Okamoto E. Prediction of hemolysis in rotary blood pumps with computational fluid dynamics analysis. *J Congestive Heart Failure Circ Support* 2001;1:331–6.
3. Kawano S, Yamakami J, Kamijio K, Hashimoto H, Yambe T, Nitta S. Computational design of vibration pumping device for artificial heart. *Trans ASME J Pressure Vessel Technology* 2001;123:525–9.
4. Wood HG, Anderson J, Allaire PE, McDaniel JC, Bearnson G. Numerical solution for blood flow in a centrifugal ventricular assist device. *Int J Artif Organs* 1999;22(12):827–36.
5. Anderson JB, Wood HG, Allaire PE, McDaniel JC, Olsen DB, Bearnson G. Numeric studies of blood shear and washing in a continuous flow ventricular assist device. *ASAIO J* 2000;46:486–94.
6. Miyazoe Y, Sawairi T, Ito K, Konishi Y, Yamane T, Nishida M, Masuzawa T, Takiura K, Taenaka Y. Computational fluid dynamic analyses to establish design process of centrifugal blood pumps. *Artif Organs* 1998;22:381–5.
7. Apel J, Paul R, Klaus S, Siess T, Reul H. Assessment of hemolysis related quantities in a microaxial blood pump by computational fluid dynamics. *Artif Organs* 2001;25:341–7.
8. Giersiepen M, Wurzinger LJ, Opitz R, Reul H. Estimation of shear stress-related blood damage in heart valve prostheses—in vitro comparison of 25 aortic valves. *Int J Artif Organs* 1990;13:300–6.
9. Bludszuweit C. Three-dimensional numerical prediction of stress loading of blood particles in a centrifugal pump. *Artif Organs* 1995;19:590–6.
10. Bludsuweit C. Model for a general mechanical blood damage prediction. *Artif Organs* 1995;19:583–9.
11. Treichler J, Rosenow SE, Damm G, Naito K, Ohara Y, Mizuguchi K, Makinouchi K, Takatani S, Nosé Y. A fluid dynamic analysis of a rotary blood pump for design improvement. *Artif Organs* 1993;17:797–808.
12. Yeleswarapu KK, Antaki JF, Kameneva MV, Rajagopal KR. A mathematical model for shear-induced hemolysis. *Artif Organs* 1995;19:576–82.

Artificial Organs
27(10):892–896, Blackwell Publishing, Inc.

Development of a Magnetic Fluid Shaft Seal for an Axial-Flow Blood Pump

*Kazumitsu Sekine, *Yoshinori Mitamura, *Shun Murabayashi, *Ikuya Nishimura, †Ryouhei Yozu, and ‡Dong-Wook Kim

**Hokkaido University, Sapporo, Hokkaido, Japan; †Keio University; and ‡Soonchunhyang University, Asan, Chungnam, Korea*

Abstract: A rotating impeller in a rotary blood pump requires a supporting system in blood, such as a pivot bearing or magnetic suspension. To solve potential problems such as abrasive wear and complexity of a supporting system, a magnetic fluid seal was developed for use in an axial-flow blood pump. Sealing pressures at motor speeds of up to 8,000 rpm were measured with the seal immersed in water or bovine blood. The sealing pressure was about 200 mm Hg in water and blood. The calculated theoretical sealing pressure was about 230 mm Hg. The seal remained perfect for 743 days in a static condition and for 180+ days (ongoing test) at a motor speed of 7,000 rpm. Results of measurement of cell growth activity indicated that the magnetic fluid has no negative cytological effects. The specially designed magnetic fluid shaft seal is useful for an axial-flow blood pump. **Key Words:** Axial-flow blood pump—Magnetic fluid seal—Sealing pressure—Biocompatibility.

Nowadays, several implantable continuous-flow artificial heart systems have been developed, and some have already been used clinically. We have been developing an axial-flow blood pump as a left ventricular assist device (1). The rotating impeller in a rotary blood pump requires a supporting system. A pivot bearing is used in magnetic coupling systems, but it causes hematological problems such as thrombus formation or hemolysis because of its mechanical contact and heat generation. Recently, magnetic suspension has been used in several rotary blood pumps, but it requires a power-consuming and large-scale control system because of electromagnetic coupling.

To solve potential problems in current systems, we have been studying the possibility of application of a magnetic fluid seal as a seal system for rotary blood pumps. Magnetic fluid is a mixture of ferromagnetic nanoparticles and solvent. The magnetic properties of a magnetic fluid depend on the characteristics of the ferromagnetic particles, and the chemical properties depend on the characteristics of the solvent. Magnetic fluid has recently been studied for clinical applications, for example, as a heat generator of hyperthermia (2) and as a drug transporter for drug delivery systems (3). Several biocompatible magnetic fluids have been developed (4–6). A magnetic fluid seal has several advantages. It has a high degree of airtightness because the magnetic fluid seal is formed with liquid. There is no wear because of its noncontact structure with any solids. It generates very low frictional heat and noise. It does not require external power for the seal itself. One of its best characteristics is its very simple structure. However, a magnetic fluid seal also has some potential problems. One problem is its relatively low sealing pressure. Magnetic fluid seals have generally been used in precision machines for protection against dust and have not been used as liquid seals because of the relatively low sealing pressure of magnetic fluid seals compared to that of mechanical seals. For use in a blood pump, a magnetic fluid seal must have a sufficient level of sealing pressure to enable maintenance of a seal

Received June 2003.
Address correspondence and reprint requests to Dr. Kazumitsu Sekine, Department of Biomedical Systems Engineering, Division of Systems and Information Engineering, Graduate School of Engineering, Hokkaido University, Kita 13 Nishi 8, Kita-ku, Sapporo 060-8628, Japan. E-mail: seki777@bme.eng.hokudai.ac.jp
Presented in part at the 10th Congress of the International Society for Rotary Blood Pumps, held September 11–14, 2002 in Osaka, Japan.

against normal blood pressure. Another problem with this seal system is the loss of the magnetic fluid. If the amount of loss of magnetic fluid is large, the seal will not continue to work for a long time, and if a large amount of magnetic fluid is mixed, side effects of the magnetic fluid, such as toxicity, will limit its clinical use.

In this study, therefore, we have examined in detail the three potential problems of sealing pressure, durability, and biocompatibility of a magnetic fluid seal system. Sealing pressure was measured using water and bovine blood, and was also theoretically calculated using a magnetic finite element method. The durability of the seal system was tested in rotational and static shaft conditions. Finally, in vitro biocompatibility tests, that is, cytotoxicity tests, were carried out using mammalian cells.

MATERIALS AND METHODS

Structure of the magnetic fluid seal

A schematic structure of the magnetic fluid seal is shown in Fig. 1. The magnetic fluid seal has a cylindrical structure and is composed of a permanent magnet (NEOMAX41, Nd-Fe-B, Sumitomo Special Metals, Osaka, Japan) sandwiched between two polepieces. The magnet is 8 mm in outer diameter, 3.6 mm in inner diameter, and 1 mm in thickness. Each polepiece is 8 mm in outer diameter, 3.1 mm in inner diameter, and 0.5 mm in thickness. The shaft is 3 mm in diameter. The permanent magnet is axially magnetized, and the two polepieces and the shaft are ferrostainless (SUS420). A seal is formed by injecting magnetic fluid into the gap (50 μm) between the polepieces and the shaft. The injected magnetic fluid is suspended in place by the force of a magnetic field. The magnetic fluid used in this study was Ferricolloid

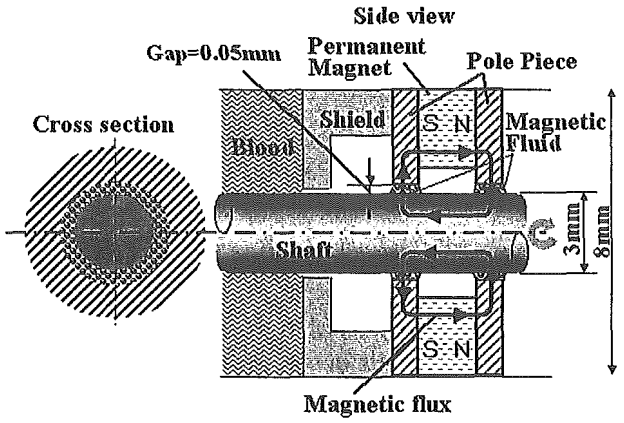

FIG. 1. Schematic structure of the magnetic fluid seal.

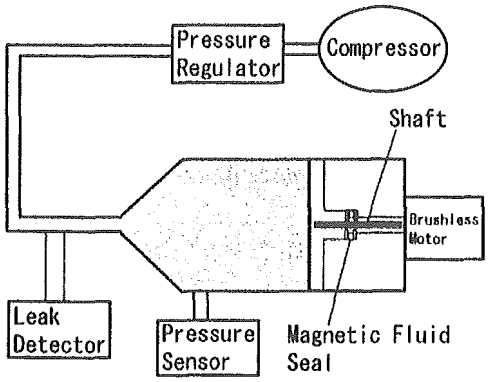

FIG. 2. Apparatus for sealing pressure measurement.

LS-40 (Taiho Industrials, Kanagawa, Japan; saturation magnetization: 24.3 kA/m). The ferromagnetic nanospheres dispersed in LS-40 are magnetite (Fe_3O_4) particles with a uniform size distribution in a range of nanometer order, and the solvent is alkyl-naphthalene. Weight (or volume) percentages of the magnetite, alkyl-naphthalene, and surfactant of LS-40 are about 40%, 55%, and 5%, respectively. The iron oxides normally used in magnetic fluid, magnetite and maghemite, are insoluble in blood and inert in the human body.

Sealing pressure

The apparatus used for sealing pressure measurement is shown in Fig. 2. The magnetic fluid seal was installed on the shaft of a DC brushless motor (EC22, Maxon Japan, Tokyo, Japan). The seal assembly was fixed to the casing. In this study, 15 μl of magnetic fluid was used. The case was filled with water or bovine blood to which citrate phosphate dextrose had been added. The motor speed was changed from 0 to 8,000 rpm every 1,000 rpm. The seal was pressurized with a compressor (AC0910, MEDO, Tokyo, Japan), and the pressure was monitored and recorded with a pressure sensor (P23XL, Ohmeda Medical Devices Division, Madison, WI, U.S.A.) and a digital recorder (RT3424, NEC San-ei, Tokyo, Japan). The pressure was increased gradually until the seal failed. When the seal fails, the pressure drops rapidly. The pressure at that point was defined as the sealing pressure at that motor speed.

Theoretical sealing pressure was calculated by analyzing the magnetic field in the seal model. The seal was modeled as a two-dimensional axis-symmetrical model, and the intensity of the magnetic field was calculated by using a magnetic finite element method (ANSYS/University High, ANSYS, Canonsburg, PA, U.S.A.). The magnetic properties of the shaft, polepieces (SUS420), and magnetic fluid were used in the

FEM model. The B-H curve of a permanent magnet (Br = 1.28 T, Hc = 1,140 kA/m) was used in the model. The seal pressure is given as follows (7,8):

$$\zeta = \frac{\text{shaft radius}}{\text{pole piece inner radius}} = \frac{r_0}{r_1}$$

$$b^2 = \frac{\zeta^2}{(1-\zeta^2)}$$

$$\Psi(r) = \frac{1}{2}\left\{r^2 - 4r_1^2 \ln\left(\frac{r}{r_1}\right) - \frac{r_1^4}{r^2}\right\}$$

$$\chi = \frac{C_\beta \rho \Psi(r_0)}{(\zeta^{-4}-1)}$$

$$\Delta p = NkT \ln\left(\frac{\xi_{11}\sinh\xi_{00}}{\xi_{00}\sinh\xi_{11}}\right) + \omega_s^2 b^4 \{\rho\Psi(r_0) - \chi(\zeta^{-4}-1)\} \quad (1)$$

where

$$\xi_{nn} = mH_{nn}/kT, \quad (2)$$

m is the magnetic moment of a particle, N is the number density of particles, k is the Boltzmann constant, T is temperature of the magnetic fluid, ω_s is the angular velocity, C_β is the non-Newtonian coefficient, r_0 is the radius of the rotating shaft, r_1 is the radius of the seal, and ξ_{00}, ξ_{11} are the values calculated from the intensities of the magnetic fields inside (H_{00}) and outside (H_{11}) the magnetic fluid, respectively. The values of magnetic fields calculated in magnetic FEM analysis were substituted into Eq. 2. Then, values of ξ were substituted into Eq. 1. The first term in Eq. 1 represents the effect of a magnetic field and the second term represents the effect of a rotating shaft. In these equations, the effect of rotational speed of the shaft on the seal pressure was taken into account in the calculation of the second term.

Long-term durability

The apparatus used for testing long-term durability was the same as that used for sealing pressure measurement. The case was filled with distilled water. One test was conducted under a static condition and two tests were conducted at a speed of 7,000 rpm. In the static test, 15 µl of magnetic fluid was used in the seal, and a pressure of 100 mm Hg (13.3 kPa) was applied to the seal. In the rotational tests, 10 µl of magnetic fluid was used. The pressure loads were 100 mm Hg in the first test and 150 mm Hg (20 kPa) in the second test.

Biocompatibility

Murine fibroblast-derived L929 cells were used for toxicological evaluations. L929 cells were purchased from Dainihon Pharmaceutical (Osaka, Japan). The cells were suspended to a final density of 0.2×10^5 cells/ml or 1.0×10^5 cells/ml in Eagle's minimum essential medium (ICN Biomedical, Aurora, OH, U.S.A.) containing 10% heat-inactivated FBS, 50 U/ml penicillin, and 50 µg/ml streptomycin. They were incubated at 37°C in a 5% CO_2/95% air humidified environment in the presence of 10 µl/ml magnetic fluid (LS-40) or the solvent of magnetic fluid (alkyl-naphthalene, Lion, Tokyo, Japan). LS-40 and alkyl-naphthalene were sterilized by filtration through a membrane filter of 0.22 µm pore size (Millex-GV, Japan Millipore, Tokyo, Japan) before use. The cell suspension of 1.0×10^5 cells/ml was incubated for 96 hr (experiment 1), and the cell suspension of 0.2×10^5 cells/ml was incubated for 1 week (experiment 2). After incubation, the cells were isolated by trypsin treatment and counted under a phase-contrast microscope. Cell viability was assessed by trypan blue exclusion. The number of viable cells was compared with that of viable control cells cultured in the absence of LS-40 or the solvent.

RESULTS

Sealing pressure

The results of sealing pressures at different motor speeds are shown in Fig. 3. A sealing pressure of about 200 mm Hg was obtained at all motor speeds, and the sealing pressure of stage 3 and stage 4 seals were 100–150 mm Hg higher than those of other seals.

Long-term durability

The durability test carried out in a static motor condition was continued for up to 2 years (743 days: electively terminated). The seal remained perfect for a period of 96 days at 7,000 rpm. The test was terminated due to motor fixation failure. Another seal has remained perfect for 180 days as of October 23, 2002 and the test is still ongoing.

Biocompatibility

Cell concentrations before and after incubation are shown in Fig. 4. Negative cytological effects due to the organic compound solvent of magnetic fluid or the magnetic fluid itself were not observed from cell growth activities in experiments 1 and 2. No significant difference was found between cell counts in the control and the culture with solvent or between cell counts in the control and the culture with the magnetic fluid. The shape of the cells was identical to that of the control cells after incubation, and no significant difference in morphological

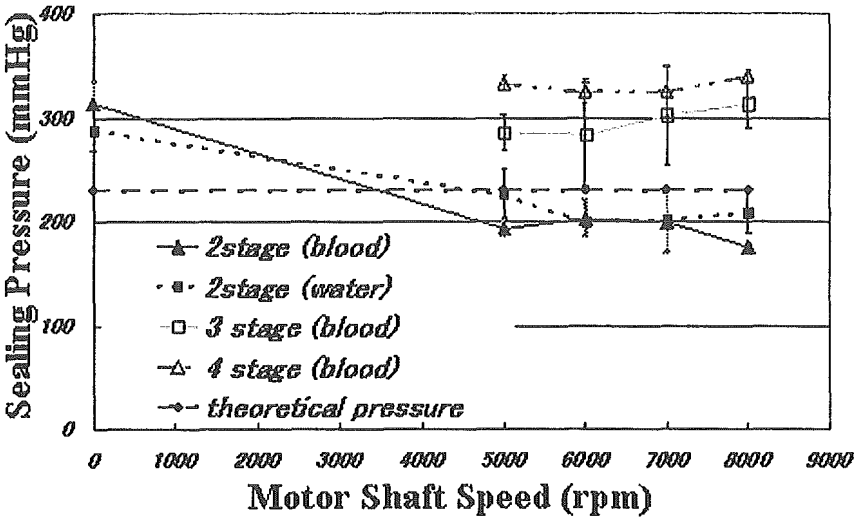

FIG. 3. Results of sealing pressure measurements at various motor speeds.

observation was found between pre- and postincubation by trypan blue stain assay.

DISCUSSION

A magnetic fluid seal has several advantages, but it also has several potential problems if it is to be used in a clinical rotary blood pump. In this study, these potential problems were examined in detail. A level of sealing pressure was sufficiently high to enable maintenance of the seal against normal blood pressure. And, the use of a multistage seal increased the sealing pressure further. Sufficient sealing pressure will be obtained by further development of magnetic fluid seal structure and magnetic characteristics of magnetic fluid.

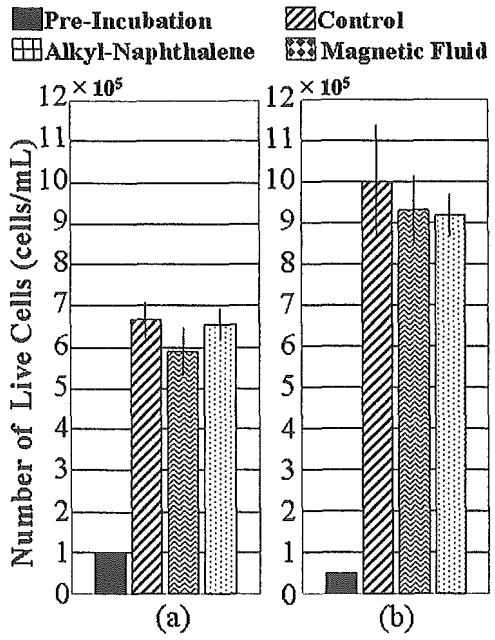

FIG. 4. Results of cytotoxicity study. (a) Cell concentrations before and after incubation in experiment 1. (b) Cell concentrations before and after incubation in experiment 2. In both experiments, a control, a culture with solvent, and a culture with magnetic fluid were used. No significant difference was found between the control and the culture with solvent or between the control and the culture with magnetic fluid.

One of the key factors for applicability of this seal system is its long-term performance. The results of the long-term durability test have shown that the seal remains perfect for a period of 6 months, and this test is still ongoing. It is expected that the durability of the seal system is much longer than 6 months. The characteristics of the magnetic fluid seal were not examined under the condition of variable motor speed in this study. However, in clinical use, the motor speed of the blood pump will be changed to maintain physiological cardiac output. And, in the clinical situation of an axial-flow blood pump such as a VAD, the pressure difference across the pump changes during a cardiac cycle due to the changes in left ventricular and aortic pressures. Further studies are planned to study the performance of the magnetic fluid seal under the conditions of variable motor speeds and pulsatile changes of pressure load.

Toxicity of the magnetic fluid must be carefully studied before clinical applications, because mixing of the magnetic fluid and blood may occur. The results of biocompatibility tests of the magnetic fluid showed normal cell growth activity and no toxic effect of the magnetic fluid. Moreover, our previous study showed that the amount of magnetic fluid that leaked over a period of 14 days was less than 1 μl and that there was no further leakage of magnetic fluid

(9). Further tests should be carried out to verify the safety of the magnetic fluid seal, but the results of this study indicate that the toxicity of the current magnetic fluid seal is not a major issue.

From another point of view, the vibration of the shaft is one of the most critical problems. A non-direct drive pump, that is, magnetic suspension, must consider this point, which is caused by the movement of patients. In our pump, the magnetic fluid seal suspends the shaft stably through the axis-symmetric magnetic force. This advantage would improve by the use of higher magnetic properties of magnetic fluid. The magnetic fluid seal is a very useful lubricated bearing.

CONCLUSIONS

A magnetic fluid seal was specially designed for use in an axial-flow blood pump. The sealing pressure was about 200 mm Hg in blood. The results of a long-term durability test showed that the durability of the seal was more than 6 months. The results of biocompatiblity tests showed that the magnetic fluid had no major problems in clinical applications. The results of this study indicate that this simple biocompatible liquid seal, which does not require power, is useful for a rotary blood pump.

Acknowledgments: This study was supported in part by a Grant-in-Aid for Scientific Research from the JSPS (no. 14380386).

REFERENCES

1. Mitamura Y, Nakamura H, Okamoto E, Yozu R, Kawada S, Kim DW. Development of the valve pump: an axial flow pump implanted at the heart valve position. *Artif Organs* 1999;23: 566–71.
2. Jordan A, Scholz R, Maier-Hauff K, et al. Presentation of a new magnetic field therapy system for the treatment of human solid tumors with magnetic fluid hyperthermia. *J Magn Magn Mater* 2001;225:118–26.
3. Lubbe AS, Bergemann C, Brock J, McClure DG. Physiological aspects in magnetic drug-targeting. *J Magn Magn Mater* 1999; 194:149–55.
4. Gansau C, Buske N, Gross C, Weitchies W. Novel biocompatible magnetic fluids. *Eur Cell Mater* 2002;3:158–9.
5. Petri A, Chastlellain M, Hofmann H, Rao KV. Investigation of ferrofluids for biomedical application. *Eur Cell Mater* 2002;3: 183–4.
6. Lacava LM, Lacava ZGM, Da Silva MF, et al. Magnetic resonance of a dextran-coated magnetic fluid intravenously administered in mice. *Biophys J* 2001;80:2483–6.
7. Nagaya K, Ohnuma H, Sato A. Analysis of a radial magnetic fluid seal and a radial bearing lubricated with a magnetic fluid. *Tribol Int* 1992;25:107–13.
8. Kamiyama S, Oyama T, Htwe J. Basic study on the performance of magnetic fluid seal. *Proc JSLE Int Tribol Conf* 1985;985–90.
9. Sekine K, Asakawa M, Mitamura Y. Development of an axial flow blood pump: characteristics of a magnetic fluid seal. *J Artif Organs* 2001;4:245–51.

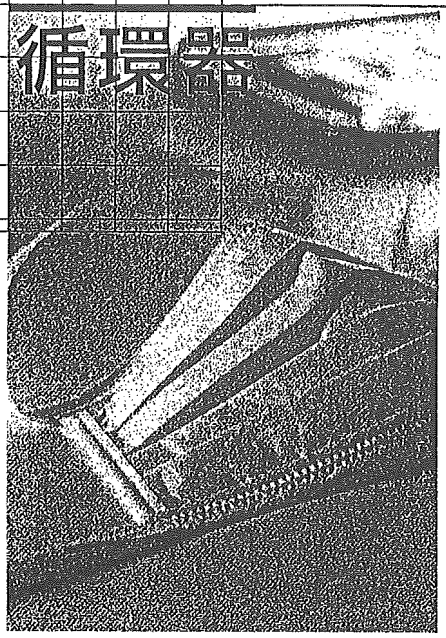

弁膜症手術の最前線；最新の適応とは？

低侵襲心臓弁膜症手術の最前線

Port-Access MICSからロボット支援下心臓手術まで

飯野 与志美（慶應義塾大学医学部心臓血管外科）
申　　範圭（慶應義塾大学医学部心臓血管外科講師）
四津　良平（慶應義塾大学医学部心臓血管外科教授）

Point ☞

- ●弁膜症における低侵襲心臓手術（MICS）は、Cosgroveらの右傍胸骨切開大動脈弁手術に始まる。
- ●1997年には、ChitwoodらによりPort-Acccessの新しい手法を取り入れた右小開胸での内視鏡下僧帽弁手術が報告され、この時期からこの手法が、①低侵襲、早期回復、②医療コストの削減、③美容効果などを目指して行われるようになった。
- ●さらに最近では、その手術技術が新しいコンピュータ技術と結びつき、完全内視鏡下での手術を目指したMaster-Slave manipulatorによる手術、いわゆるロボット手術が行われるようになった。
- ●臨床応用されている2種類のロボットではいずれも成功例が報告されている。
- ●わが国ではまだまだ広まっているとはいえないMICSであるが、患者の肉体的・精神的負担の軽減、医療費削減が求められている現在、これらの技術が心臓外科手術法の1つのオプション、あるいはメニューになっていくことは確実であると考えられる。

低侵襲心臓手術の発展

1980年代に消化器外科領域で腹腔鏡下胆嚢摘出術が開発されて以来、内視鏡下もしくは小切開手術が単に傷を小さくするという美容的な結果だけでなく、手術後の社会復帰も早く、また医療コストの削減にもつながることより、いろいろな手術領域において低侵襲手術あるいは内視鏡下手

0910-0474/03/￥400/論文/JCLS

術が検討されるようになった。

心臓血管外科領域では、心房中隔欠損手術においては本来の手術手技が単純であるため、比較的早期より美容的な立場から皮膚切開の工夫がされている。1980年頃から、乳房下に沿って皮膚切開し胸骨正中切開を行う方法や、皮膚切開を短縮した胸骨正中切開や、右乳房下に沿って皮膚切開を行い第4肋間開胸による手術が報告されている。しかし、これらは低侵襲手術ということは特に意識しておらず、単に美容的効果を狙ったものであった。低侵襲を意識した手術は、1995年にBanettiらが発表したminimally invasive direct coronary artery bypass (MIDCAB) が最初である[1]。

弁膜症における低侵襲心臓手術は、Cosgroveらが右傍胸骨切開にて大動脈弁手術を行ったのが最初である。1997年にはChitwoodらが第4肋間開胸および第5肋骨部分切除にて僧帽弁手術を行い、さらにCosgroveらは胸骨横断法によるアプローチを発表し、同年にPort-Acccessの新しい手法を取り入れた右小開胸での内視鏡下僧帽弁手術 (micro-mitral operation) を報告した[2]。この時期からPort-Access法による心臓手術が、①低侵襲、早期回復、②医療コストの削減、③美容効果などを期待できる手術として行われるようになった。さらに最近では、その手術技術が新しいコンピュータ技術と結びつき、完全内視鏡下での手術を目指したMaster-Slave manipulatorによる手術、いわゆるロボット手術が行われるようになり、心臓外科領域でも手術用ロボットを用いた低侵襲心臓手術が行われるようになった。

現在、臨床応用されている手術用ロボットには、米国Intuitive Surgical社のda VinciとComputer Motion社のZeusがあり、いずれも成功例が報告されている[3,4]。

ここでは、低侵襲心臓手術、主にPort-Access僧帽弁膜症手術について述べる。

A. Intracardiac repair (心臓内修復) : valve, ASD, et al
standard MICS (parasternotomy, ministernotomy, et al)
Port-Access MICS (single or multiple ports)
EAC (end aortic clamp) balloon
Heartport system
direct EAC (Yozu balloon)
AXC (aortic cross clamp)
Chitwood sliding clamp
Cosgrove flex clamp
modified Cosgrove flex clamp (Cosgrove-Yozu)
B. Coronary artery bypass graft (冠動脈バイパス移植)
standard MICS (ministernotomy, et al) on pump
OPCAB (off pump coronary artery bypass)
MIDCAB (minimally invasive direct coronary artery bypass)
LAST (left anterior small thoracotomy)
TMR (transmyocardial laser revascularization)
C. Robotic cardiac surgery (ロボット心臓手術)
ASD, mitral valve (on pump)
CABG (on pump or off pump)

表1 MICSの分類

低侵襲心臓手術 (MICS) の定義

現在われわれは、①体外循環を使用しないこと、②胸骨全長切開を行わないこと、③またはその両方、これらのいずれかの条件を満たすものを低侵襲心臓手術 (minimally invasive cardiac surgery；MICS) と考えている。MICSの分類を表1に示す。Port-Access心臓手術は、低侵襲心臓手術法 (MICS) のなかの一つであり、従来の胸骨正中切開に代わり、単一または複数のport (s) (小切開創) から心臓に到達する心臓手術法の総称である[5]。

MICS手術における僧帽弁手術の切開法(図1)

① Mini-sternotomy with lower right-side semi-transverse division (J字法)

Standard MICSでは第2肋間 (2nd J字法) で切開しており、Port-Access MICSでは大動脈遮断法の工夫により

第3肋間以下でのほんのわずかの胸骨切開で手術ができるようになった（図1a）。なお第3肋間以下の切開（3rd J字法）では上行大動脈へのアプローチは不可能である。

②右乳房下切開

これは右乳房下に5～7cmの皮膚切開を行い、第4肋間にてミニ開胸する（図1b）。肺をcollapseさせ心膜を切開すれば、右房および右側左房が露出する。

これらの切開法による僧帽弁手術は、手術視野が小さく、また僧帽弁の位置は非常に深くなる。そのため内視鏡を用いて深い術野を拡大してモニターする工夫や、複雑な操作を容易に行うための内視鏡手術器具が開発されている。

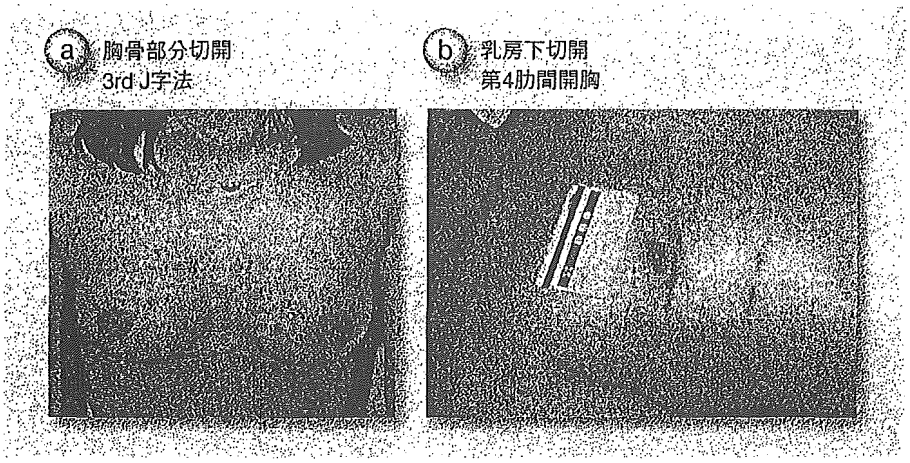

図1　Port-Access MICSの術創

MICSのための体外循環の工夫

低侵襲の意味からすると体外循環を使用しないことが望ましいが、現時点では弁膜症の心臓手術は体外循環なしには不可能である。ここではMICSに適した体外循環の工夫について説明する。

1．カニューレ

Central CPBの場合、小さな手術視野で手術を行うため、小口径のカニューレが適している。Peripheral CPBの場合は術野にカニューレがないため、視野的に有利である。

2．脱血の工夫

MICSの手術創においてはPeripheral CPBの方が望ましいが、主に脱血不良にてポンプ流量に脱血量が追いつかないことがある。通常脱血は落差脱血で行われているが、細いカニューレからより多くの流量を出すために種々の方法が考えられている。VAVD（vacuum assited venous drainage）は静脈貯血槽に陰圧をかけて脱血を行う方法である。流量はカニューレの抵抗により変化するが、圧力が一定しているのでCollapse現象が起こらない。われわれはこの方法を用いており、満足のいく結果を出している。

3．大動脈遮断方法

Port-Access心臓手術では胸壁にある1つの小切開および複数のポートが唯一の心臓に到達する経路であるため、心臓停止のための上行大動脈遮断は、通常使われている遮断鉗子では行えない。そこで開発された大動脈遮断には大きく分けて2通りの方法がある。①血管内腔から遮断する方法（endoaortic clamp法；EAC法）、②血管外壁から遮断鉗子を用いて行う方法（aortic cross clamp法；AXC法）である。

①Endoaortic Clamp（EAC）法

この方法に用いるバルーンには、米国Heartport社で開発されたHeartportシステムによるものがある。バルーンを下肢末梢動脈から挿入し、上行大動脈まで進め、バルーンを膨らませ血流を遮断する。順行性の心筋保護液の注入やaortic ventが可能である。また、われわれは小切開創から上行大動脈に直接挿入できるdirect EACバルーンを独自に開発し使用している。

②Aortic Cross Clamp（AXC）法

低侵襲心臓手術用の特別な大動脈遮断鉗子で上行大動脈を遮断する方法である。胸壁に空けたportより大動脈を遮断することは、通常の遮断鉗子ではできないため、それに適した工夫された血管遮断鉗子が開発されている。現在Chitwood sliding clampと、血管遮断鉗子の柄（シャフト）の部分が自由自在に曲がるCosgrove flex clampがある。

僧帽弁へのアプローチ (図2)

左心ベントとして右上肺静脈から左室までベントカテーテルを挿入する。ここで、術野に二酸化炭素(CO_2)ガスを2L/minの流量で常時流しておく。心房間溝上の脂肪を剥離し、より僧帽弁に近い右側左房切開で左房に到達する。次にこの切開孔からatrial retractorを中隔に掛けて上方に牽引し、僧帽弁を展開する。

僧帽弁が展開されたあとは、内視鏡手術器具を用いて弁形成術を行う。ロボット心臓手術da Vinci™を用いた手術では、この段階をロボットのエンドリスト(2本の手)が行うようになる。弁形成終了後、必要であれば左房を閉鎖縫合した後、心臓停止下の状態で一時的ペースメーカー・リードを右室に縫着する。心臓が拍動開始後では止血確認は困難となるため、一時的ペースメーカー・リード装着刺入部心筋からの出血がなくても、刺入部位は5-0ナイロンで止血しておく。ドレーンは胸腔にポルトバッグを通常1本のみ挿入する。

MICSにおけるロボットの導入 ～da Vinci™を用いた心臓手術

1. da Vinci™システム(図3、4)

da Vinci™システムは、①オペレーターがロボットを実際に操作する場所である術者コンソール、②実際に手術を行う部分で内視鏡とロボットの左右の腕(アーム)をもつ手術アームカート、③コンソールでオペレーターが見ている内視鏡の高画質立体(3D)画像を外部に映し出すビジョンシステム(モニター)、の3つの部分から構成されている。術者コンソールは患者のいる場所と離れており、別室に設置することも可能である。したがってオペレーターは静かな場所で手術に集中することができる。

2. ロボット心臓手術の実際

全身麻酔、体位のセッティング、人工心肺の準備が整ったところで、ロボット心臓手術は導入される。手術種類によって、また各施設によってロボットが実際の手術のうちのどの程度を担うかはさまざまであるが、現在の主な役割としては、僧帽弁形成術の心内修復術や、冠動脈バイパス術での内胸動脈採取、血管吻合術などがあげられる。1997年3月～2001年6月の間に行われたda Vinci™を用いた心臓手術は2,094例であり、その内訳は冠動脈バイパス術での内胸動脈採取が1,171例、血管吻合術495例、僧帽弁膜症手術112例、心房中隔欠損閉鎖術35例である。

MICS手術による患者のメリット

体外循環を行わないことが低侵襲であることは理解しやすいが、心停止を伴う心臓手術に手術創を小さくすることがどれだけ低侵襲に貢献するかを評価するのは困難である。しかし、WaltherらはMICSによる手術を施行した患者の調査において、平均入院期間の短縮や創痛の軽減されたことを報告しており、澤らはMICS手術において体外循環離脱時の血中IL-8の濃度が有意に低かったと報告している。われわれのPort-Access手術経験でも平均入院期間の短縮、入院コスト

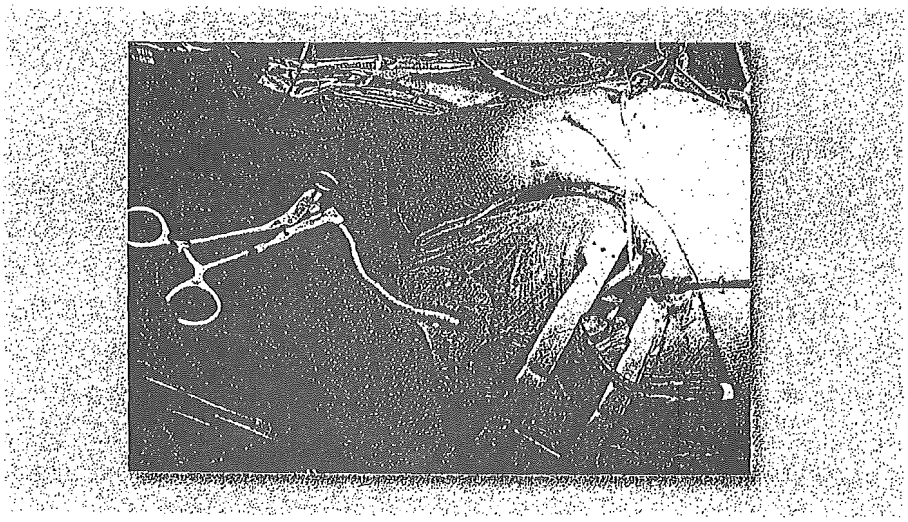

図2 Port-Access法

MICSにおける僧帽弁手術術野(遠景)。アプローチは右第4肋間から5cmの皮膚切開で行っている。

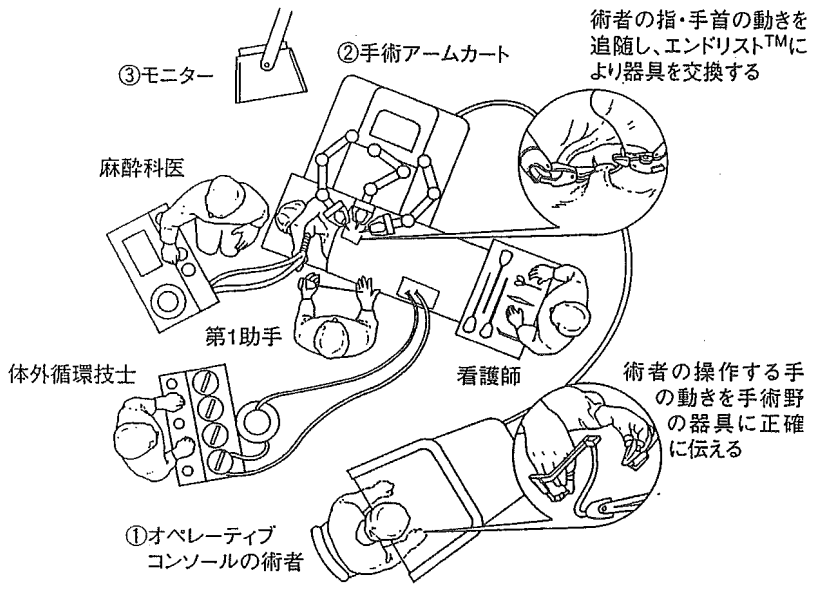

図3　da Vinci™システム
(Intuitive Surgical, Inc, Mountain View, Calif)
外科用ロボットシステム患者側の手術アームカートの中央アームに装着された内視鏡により、オペレーティブコンソールに術野が映し出される。術者はコンソールに座り、映し出された術野を見ながらレバーを操作し、手術アームカートのアームを動かす。第1助手は手術器具の交換などを担当する。

図4　da Vinci™による弁形成術術野

の軽減、術後の早期就業が確認されている。

MICSにおける今後の展望

わが国においては、MICSが欧米ほど広く行われていないことは事実である。そして伝統的な開心術の習得後に新たなMICSのためのlearning curveがあることも事実である。しかしながら、患者サイドに立った医療が求められ、その結果、患者の肉体的・精神的負担の軽減を目的とする低侵襲手術への志向が強くなり、医療経済からみて効率的な医療、すなわち回復期間が短く医療費削減に効果がある医療が求められている現代において、これらの技術が心臓外科手術法の1つのオプション、あるいはメニューになっていくことは確実であると考えられる。今後の技術革新によりさらなる発展がなされ、多くの患者に利益がもたらされることを期待したい。

文献

1) Benneti FJ, Ballester C, Sani G, et al: Video-assisted coronary bypass surgery. J Card Surg 10: 620-625, 1995.
2) Chitwood WR Jr, Elbeery JR, Chapman WH, et al: Video-assisted minimally invasive mitral valve surgery: The "Micro-Mitral" operation. Thorac Cardiovasc Surg 113: 413-414, 1997.
3) Kappert U, Cichon R, Schneider J, et al: Closed-chest coronary artery surgery on the beating heart with the use of a robotic system. J Thorac Cardiovasc Surg 120: 809-811, 2000.
4) Mohr FW, Falk V, Diegeler A, et al: Computer-enhanced "robotic" cardiac surgery: experience in 148 patients. J Thorac Cardiovasc Surg 121: 842-853, 2001.
5) 四津良平: Port-Access法による弁膜症を中心とした心内修復術.『低侵襲心臓手術』, 2002, p146-155.

TOPICS
トピックス

陰圧吸引補助脱血体外循環の有効性と問題点

－3学会合同陰圧吸引補助脱血体外循環検討委員会報告書より－

3学会合同陰圧吸引補助脱血体外循環検討委員会が設置され，陰圧吸引補助脱血の歴史と臨床的意義，アンケート調査から見た陰圧吸引補助脱血法の現状，模擬回路を用いた陰圧吸引補助脱血法の検討，陰圧吸引補助ライン内に設置されたフィルターに関する検討，安全な陰圧吸引補助脱血法に向けての提言，が行われた．その結果に基づき，①陰圧吸引補助ラインにはガスフィルターを使用せず，ウォータートラップを装着する，②陰圧吸引補助ラインは毎回滅菌された新しい回路を使用する，③貯血槽には陽圧アラーム付きの圧モニター並びに陽圧防止弁を装着する，④陰圧吸引補助を施行する際には微調整の効く専用の陰圧コントローラーを使用する，ことの4項目が平成15年3月2日に中間報告として勧告された．

埼玉医科大学心臓血管外科
許　俊鋭
KYO, Shunei

東京大学医学部心臓外科，呼吸器外科
高本　眞一
TAKAMOTO, Shinichi

慶応義塾大学医学部心臓血管外科
四津　良平
YOZU, Ryouhei

東京医科歯科大学先端外科治療学講座
坂本　徹
SAKAMOTO, Tohru

慶応義塾大学医用工学センター
又吉　徹
MATAYOSHI, Tohru

埼玉医科大学MEサービス部
見目　恭一
KENMOKU, Kyoichi

クリニカル エンジニアリング
Clinical Engineering

秀潤社

日本心臓血管外科学会
URL: http://jscvs.umin.ac.jp/
日本人工臓器学会
URL: http://jsao.bcasj.or.jp/
報告書は以下の6項目よりなる.

1. 始めに
2. 陰圧吸引補助脱血の歴史と臨床的意義
3. アンケート調査から見た陰圧吸引補助脱血法の現状
4. 模擬回路を用いた陰圧吸引補助脱血法の検討
5. 陰圧吸引補助ライン内に設置されたフィルターに関する検討
6. 安全な陰圧吸引補助脱血法に向けての提言

可能な限り客観的データに基づいて作成努力がなされたが，学術団体である学会の調査能力に一定の限界があり，東京女子医大の事故に関してはあくまでフィルタ目詰まりによる閉塞の可能性を示唆したにすぎない.

この検討会の目的がより安全な陰圧吸引補助脱血体外循環法の確立であることは，最終報告に先立ち平成15年3月2日に，さらなる事故を防止するために陰圧吸引補助脱血体外循環を施行する際の4項目よりなる勧告を全国の関係者に通知したことからも理解されるものと考える*.

これまで，わが国の医療事故に関してその領域の専門家が個人単位で検討し，意見陳述をしてきた事例は多々みられるが，関係学会が専門家集団を結集して問題点の解明に取り組み安全基準の確立に取り組んだ事例はほとんどみられず，今後の医療事故対策に関する取り組みの1つの方向性を示したことは画期的なことといえよう．また，この報告書は陰圧吸引補助脱血体外循環を使用する医師，操作する臨床工学技士にとって施行方法のガイドラインとなり，また患者にとっても，安全な手術を受け，術後のQOL (quality of life)の改善に役立つことを切に願って作成されたものである．本稿は，3学会合同委員会報告書に基づき，陰圧吸引補助脱血体外循環の有効性と問題点について解説を加えたものである．よって，表1，図1～図9は報告書から引用しており，また，文章も大部分報告書を抜粋したものであるが，一部著者の責任で改変を加えている.

2. 陰圧吸引補助脱血法の歴史と臨床的意義

体外循環の脱血法には，落差脱血法と，脱血ラインにポンプを組み込むポンプ補助脱血法，静脈貯血槽に陰圧をかける陰圧吸引補助脱血法がある.

陰圧吸引補助脱血法は1952年にClarkにより提唱され，1995年に小山らも心嚢内血液サクションやベント脱血を増幅する低陰圧吸引法を考案している．1997年に慶応大学の又吉，四津らが低侵襲心臓外科手術(minimally invasive cardiac surgery：MICS)の体外循環に陰圧吸引補助脱血法を用いることを提唱し，それがクリーブランド・クリニック[2),3)]に導入され世界的に普及した．又吉，四津ら[4),5),6)]は，細い脱血管を用いたり大腿静脈など末梢からのカニュレーションによる脱血を行うMICSで陰圧吸引補助脱血法がきわめて有効であることを示す一方，陰圧吸引補助脱血を安全に実施するためには，①安定した吸引設備，②陰圧表示が可能な圧力モニタ，③専用の陰圧コントローラ，安全弁(陽圧，陰圧)の装着，陰圧吸引補助ライン(大気開放ライン付き)，結露トラップなどが必須としている．その後，陰圧吸引補助脱血法の導入における注意点や安全性に関して，見目ら，

＊ この検討会と並行して，平成14年度厚生労働科学研究「医療における危険領域のリスク分析とフェイルセーフシステムに関する研究分担研究・人工心肺の安全マニュアル作成に関する研究報告書」(古瀬 彰班長)が進められ，人工心肺運転の安全基準に関する報告書が，平成15年3月に全国の病院院長に配布された.

表1　陰圧吸引補助脱血法による体外循環
(文献1より引用)

Ⅰ　有用性
1. 陰圧吸引補助脱血法が明らかに有効な手術 低侵襲心臓手術(MICS) ポート・アクセス法による心臓手術(Port-access MICS) 胸骨小切開による心臓手術(Standard MICS) 2. 大腿静脈を脱血部位に使う心臓・大血管手術 3. 小児心臓手術 4. 回路充填液の低充填量化を意図した手術(無輸血手術率の向上) 5. 通常の開心術で小口径の脱血カニューラを用いる手術
Ⅱ　注意点
1. 体外循環(人工心肺)運転技術に習熟を要する 2. 安全性を確保する各種モニタ機器が必須である

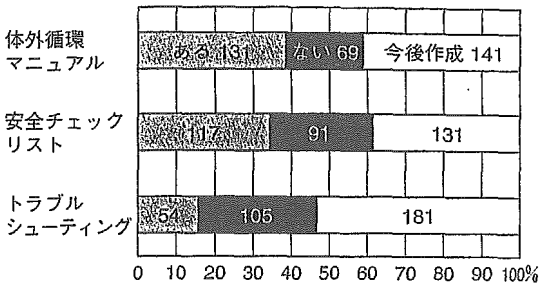

図1　体外循環業務のマニュアル整備状況
(文献1より引用)
グラフ中の数字は件数.

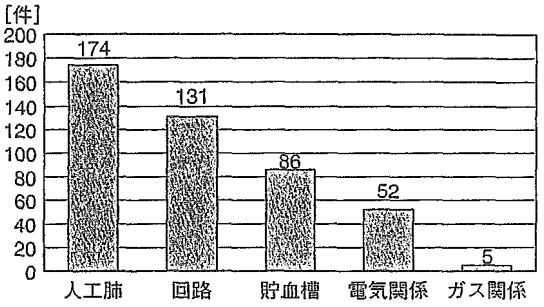

図2　インシデント・アクシデント発生部位と頻度
(文献1より引用)

山越らも十分に理解・習熟することの必要性を報告している．すなわち，陰圧吸引補助脱血においては，静脈貯血槽の陰圧が常時保たれていることの必要性と陽圧になった場合の危険性を熟知して，適切な操作方法と安全対策を講じなければならない．十分な安全対策が講じられていれば，陰圧吸引補助脱血法はMICSや大腿静脈を脱血部位に使う心臓・大血管手術，小児心臓手術，無輸血手術率の向上を目的とした回路充填液の低充填量化を意図した手術，通常の開心術でも小口径の脱血カニューレを用いる手術などに有効であり，手術の操作性を良くすることや血管損傷の回避に効果的と考えられる(表1)．

3．アンケート調査からみた陰圧吸引補助脱血法の現状

平成14年度厚生労働科学研究「医療における危険領域のリスク分析とフェイルセーフシステムに関する研究分担研究・人工心肺の安全マニュアル作成に関する研究報告書」における人工心肺のリスクに関する国内アンケート調査(平成15年3月報告書公表)は，平成14年7月に体外循環技術研究会が調査企画を立案し，同年8月3日に発足した3学会合同委員会，および同年8月27日に発足した厚生労働省研究班(古瀬　彰班長)に引き継がれ具体化したものである．

日本胸部外科学会認定・関連569施設にアンケート調査用紙が送られ，351施設(61.7%)から回答を得，回答した351施設中113(32%)施設が陰圧吸引補助脱血を施行していた．これらの施設で，2年間で494件のインシデント・アクシデント発生事例があり，年間247件となる．アンケートに回答を寄せた施設の年間手術症例数は29,279例であり，発生率は1年間に0.84%(1/119症例)であり，そのなかの陰圧吸引補助脱血関連事例は46例(9.3%)であった．寄せられた回答のなかで最大の問題は，体外循環業務のマニュアル整備状況が非常に乏しいことであった．体外循環マニュアルは38%の施設で，安全チェックリストは33%の施設でしか使用しておらず，さらに体外循環操作中何か問題が生じた場合の人工心肺危機対応手順(トラブルシューティング)は84%の施設で常備されていなかった(図1)．

インシデント・アクシデントの大部分は体外

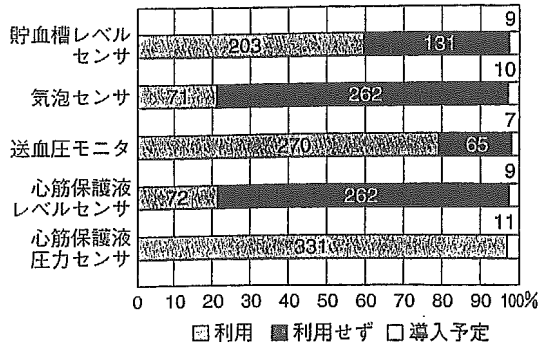

図3　安全センサ類の利用状況(文献1より引用)
グラフ中の数字は件数.

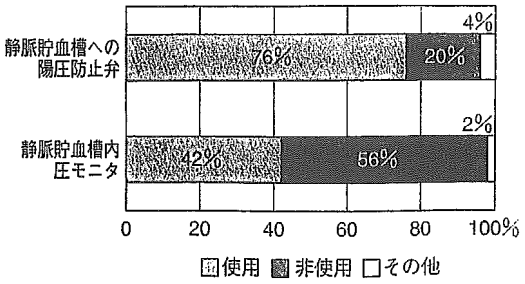

図4　陰圧吸引補助脱血時の安全対策(N＝131)
(文献1のデータより作図)

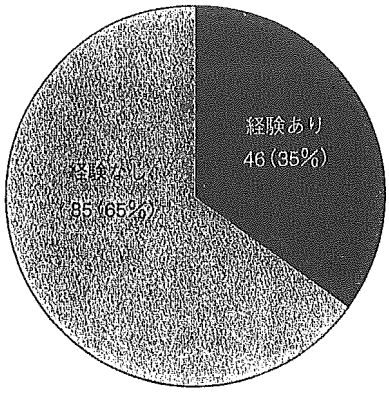

図5　陰圧吸引補助脱血時のインシデント・アクシデント(N＝131)(文献1のデータより作図)

循環回路(人工肺，回路，貯血槽)に関連したものであり，これらの防止に各種安全装置・モニタが有効であることは論を待たない(図2)．しかし，貯血槽のレベルセンサ使用施設は58%で，送血ポンプの気泡センサ使用施設は20%にすぎなかった(図3)．心筋保護液供給装置の気泡センサ使用施設は21%であり，貯血槽内の圧モニタ使用施設は42%であった．

今回の調査の要点である陰圧吸引補助脱血法に関する安全面の配慮については，貯血槽への陽圧解除弁を使用している施設は76%あり，貯血槽内の圧モニタを使用している施設は42%であった．陰圧吸引補助脱血法は体外循環に関する新しいテクノロジーであり，今後の展望として積極的に使用すると答えた施設が53%，症例によって限定使用すると答えた施設が43%あり，合わせて96%の施設が陰圧吸引補助脱血法の臨床的意義を認めていると考えられる．しかし一方，新しいテクノロジーを臨床に安全に導入するための，①チーム内の定期的なカンファレンス実施，②人工心肺マニュアルの整備，③人工心肺チェックリストの整備，④人工心肺危機対応手順の整備，など安全体制の整備は不十分である実態が明らかとなった．また，陰圧吸引補助脱血法にとって重要な貯血槽内の圧をモニタしている施設は42%にとどまり，貯血槽への陽圧解除弁を使用していない施設も24%あった(図4)．陰圧吸引補助脱血法を使用している131施設中46施設(35%)で，陰圧吸引補助脱血法にかかわる何らかのインシデント・アクシデントを経験しており(図5)，安全に陰圧吸引補助脱血法を実施するための技術習得を目的とした教育システムの確立が必要と考えられた．

4．模擬回路を用いた陰圧吸引補助脱血法の検討

陰圧吸引補助脱血法の回路構成は通常の体外循環とほぼ同じであるが，落差ではなく陰圧吸引を用いて脱血を行うため，密閉が可能な静脈貯血槽と専用の陰圧コントローラおよび陰圧吸引補助ラインが接続されている．アンケート調査でもこの陰圧吸引補助ラインには35%の施設でフィルタを装着しているが，今回，模擬回路によりフィルタを装着することが適切かどうかを検討した．また，陰圧吸引補助ラインにフィルタを装着した陰圧吸引補助脱血法を用いた東京女子医大の事故において，どのような事態が発生したのか，100回転以上のサクションやベントポ